The width of exciton formation zone dominates the performance of phosphorescent organic light emitting diodes

Weidong Sun[1,2] · Shiyu Wang[1] · Shuting Jin[1] · Xi Guan[1] · Wenxing Liu[1] · Liang Zhou[2] · Dashan Qin[1,3]

Abstract

Phosphorescent organic light emitting diodes (PHOLEDs) have been fabricated with structure of indium tin oxide/MoO$_3$ doped 4,4′-*N,N*'-dicarbazole-biphenyl (CBP) 30 nm/tris(4-carbazoyl-9-ylphenyl)amine 10 nm/CBP doped with tris(2-phenylpyridine)iridium(III) (CBP:Ir(ppy)$_3$) *x*/bathocuproine 50 nm/LiF 1 nm/Al, where $x = 2.5$, 5, 10, and 20 nm, respectively. The current efficiency (CE) of device with $x = 10$ nm is higher than those with $x = 2.5$ and 5 nm, mostly because the width of exciton formation zone (5.7 nm) with $x = 10$ nm is larger than those (2.5 and 5 nm) with $x = 2.5$ and 5 nm. However, the current density with $x = 10$ nm decreases than those with $x = 2.5$ and 5 nm at a certain driving voltage, since the ~4.3 nm CBP:Ir(ppy)$_3$ accommodating no exciton formation with $x = 10$ nm plays a role of transporting holes, raising ohmic loss of hole and thereby increasing driving voltage. When x increases from 10 to 20 nm, the width of exciton formation zone rises from 5.7 to 6.8 nm with CE almost unchanged, and the current density decreases as a result of increased ohmic loss of hole. The current research is useful to develop high-efficiency and low-driving voltage PHOLEDs.

Keywords Organic light emitting diodes · The width of exciton formation zone · Hole-electron balance · Efficiency · Driving voltage

1 Introduction

Organic light emitting diodes (OLEDs) have been broadly viewed as one of the leading flat-panel display technologies [1–10], because of their appealing properties, e.g.,

✉ Liang Zhou
zhoul@ciac.ac.cn

✉ Dashan Qin
qindashan06@aliyun.com

1 Hebei Key Laboratory of Functional Polymers, School of Chemical Engineering, Hebei University of Technology, Tianjin 300130, People's Republic of China

2 State Key Laboratory of Rare Earth Resource Utilization, Changchun Institute of Applied Chemistry, Chinese Academy of Sciences, Changchun 130022, People's Republic of China

3 Tianjin Key Laboratory of Chemical Process Safety, School of Chemical Engineering, Hebei University of Technology, Tianjin 300130, People's Republic of China

light weight, self-emission, easy fabrication on the flexible substrates, etc. In order to enter the display fields requiring high luminance and long-term stability such as augmented reality and television, OLEDs must be energy-saving, i.e., achieving high current efficiency (CE) and high luminance simultaneously at low-driving voltage (*V*). From the structural point of view, OLEDs consist of two correlated parts: the emissive layer (EML) converting charge carriers into photons and the charge transport layers delivering charge carriers from electrodes into EML.

The parameter to evaluate the emissive capability of OLED is the external quantum efficiency (EQE)

$$EQE = \gamma \times \eta_{S/T} \times \varphi \times \eta_{out}, \tag{1}$$

where γ is a factor describing hole–electron balance, $\eta_{S/T}$ represents the fraction of excitons that is allowed to decay radiatively by spin statistics, φ is the effective radiative quantum efficiency of emissive material, η_{out} is the light-outcoupling factor. The γ is defined as the probability that a hole or electron injected into EML recombines before exiting [11, 12]. By properly using electron and hole blocking layers (EBL and HBL), the γ may be advanced close to one. The $\eta_{S/T}$ equals one for phosphorescent (PH) and

thermally activated delayed fluorescent (TADF) OLEDs and 0.25 for conventional fluorescent OLEDs. The φ and η_{out} are optimized by varying the thickness of electron transport layer (ETL). The parallel orientation of emitting diodes is beneficial to η_{out} [13]. Nowadays, the values of maximum EQE for state-of-the-art PHOLEDs and TADF OLEDs have achieved $\geq 20\%$ with no additional decoration to enhance light outcoupling, approaching almost 100% internal quantum efficiencies [14–17]. Nevertheless, there are still some fundamental issues that have to be thoroughly addressed yet, for example, how the width (W) of exciton formation zone influences the performance of PHOLEDs.

The W is an important factor to underlie the performance of PHOLEDs. By employing double tris(2-phenylpyridine) iridium(III) (Ir(ppy)$_3$)-based EMLs to increase W, the EQEs of PHOLEDs have been improved [18, 19]. The layer stack of PHOLED markedly affects W [20]. The properly managed W benefits the energy transfers to realize the efficient white-light emission with stable spectra [1, 4]. Therefore, it is noteworthy to conduct more thorough work to study the effects of W on the performance of PHOLED.

Herein, the variation of W with the thickness (x) of EML, Ir(ppy)$_3$ doped 4,4′-N,N'-dicarbazole-biphenyl (CBP:Ir(ppy)$_3$), has been experimentally measured. It is found that the W increases with increase in x; with increase in W, the CE increases firstly and then becomes almost constant. The properly managed W is of importance to optimize the balance between CE and current density (J) at a given V. This work is useful to design high-efficiency and -luminance PHOLEDs with low V.

2 Experimental

The glass substrates coated with 100-nm-thick indium tin oxide (ITO) thin film were commercially available with a sheet resistance of 10 Ω per square. After cleaned in acetone, alcohol, and deionized water in sequence by an ultrasonic horn, the patterned ITO substrates were blown dry by a nitrogen gun and then treated in UV-ozone for 15 min before being loaded into the vacuum chamber. The CBP, tris(4-carbazoyl-9-ylphenyl)amine (TCTA), bathocuproine (BCP), Ir(ppy)$_3$, and bis(1-phenylisoquinoline) (acetylacetonate)iridium(III) (Ir(piq)$_2$(acac)) with purities of > 99.5% were purchased from Jilin OLED Material Tech Co., Ltd. The LiF and MoO$_3$ with purities of > 99.99% were obtained from Sigma-Aldrich Company. The Ir(ppy)$_3$ doped CBP (CBP:Ir(ppy)$_3$ by 92:8 mass ratio) was used as EML. The Ir(piq)$_2$(acac) was applied as emissive probe to detect the location of exciton formation. MoO$_3$ doped CBP (CBP:MoO$_3$ by 2:1 mass ratio) was used as hole transport layer (HTL) to facilitate hole injection and transport. The TCTA and BCP were used as EBL&HTL and HBL&ETL,

respectively. All the materials were used as received. The base pressure of the vacuum chamber for fabricating the devices by means of thermal evaporation was 5.0×10^{-4} Pa. The emissive area of device was controlled to be 8 mm^2 by patterning aluminum cathode.

PHOLEDs 1–4 with structure of ITO/CBP:MoO$_3$ 30 nm/ TCTA 10 nm/CBP:Ir(ppy)$_3$ x/BCP 50 nm/LiF 1 nm/Al, where $x = 2.5, 5, 10, 20$ nm, respectively, were fabricated to study the dependence of CE on x.

In order to detect the exciton formation in EML for PHOLEDs 1–4, a 1 nm layer of Ir(piq)$_2$(acac) was inserted between EML and BCP, resulting four probing devices (PD-BE 1–4) with structure of ITO/CBP:MoO$_3$ 30 nm/TCTA 10 nm/CBP:Ir(ppy)$_3$ x/Ir(piq)$_2$(acac) 1 nm/BCP 50 nm/ LiF 1 nm/Al, where $x = 2.5, 5, 10, 20$ nm, respectively. A 1 nm layer of Ir(piq)$_2$(acac) was also introduced between TCTA and EML, resulting four probing devices (PD-TE 1–4) with structure of ITO/CBP:MoO$_3$ 30 nm/TCTA 10 nm/ Ir(piq)$_2$(acac) 1 nm/CBP:Ir(ppy)$_3$ x/BCP 50 nm/LiF 1 nm/ Al, where $x = 2.5, 5, 10, 20$ nm, respectively.

The J–V characteristics and luminance of the devices were measured using a programmable Keithley 2400 sourcemeter and an ST-86LA spot photometer, respectively, under the air condition. The electroluminescent (EL) spectra of the devices were recorded via a L88/OPT-2000 spectrophotometer.

3 Results and discussion

3.1 The optoelectronic performance of PHOLEDs 1–4

The molecular structures of organic materials are shown in Fig. 1. The performance of PHOLEDs 1–4 is compared in Fig. 2. It can be seen that PHOLEDs 1 and 2 show comparable J-V curves, improved than those of PHOLEDs 3 and 4; the J of PHOLED 3 is increased than that of PHOLED 4 at a given V. For example, the J of PHOLEDs 1–4 is 14.1, 15.4, 10.2, 4.2 mA/cm^2, respectively, at $V = 8.0$ V. PHOLEDs 1–3 are brighter than PHOLED 4. For example, the luminance for PHOLEDs 1–4 is 2770, 3510, 3086, and 1413 cd/m^2, respectively, at $V = 8.0$ V. PHOLEDs 3 and 4 present comparable CEs at a certain J, higher than those of PHOLEDs 1 and 2; PHOLED 2 is more current-efficient than PHOLED 1. The CEs for PHOLEDs 1–4 are 27.0, 31.7, 37.3, and 36.9 cd/A, respectively, at $J = 0.1$ mA/cm^2. PHOLEDs 3 and 4 are also more power-efficient than PHOLEDs 1 and 2. The power efficiencies for PHOLEDs 1–4 are 18.1, 21.1, 23.9, and 22.0 lm/W, respectively, at $J = 0.1$ mA/cm^2. Therefore, it is conclusive that the device performance is optimized with $x = 10$ nm.

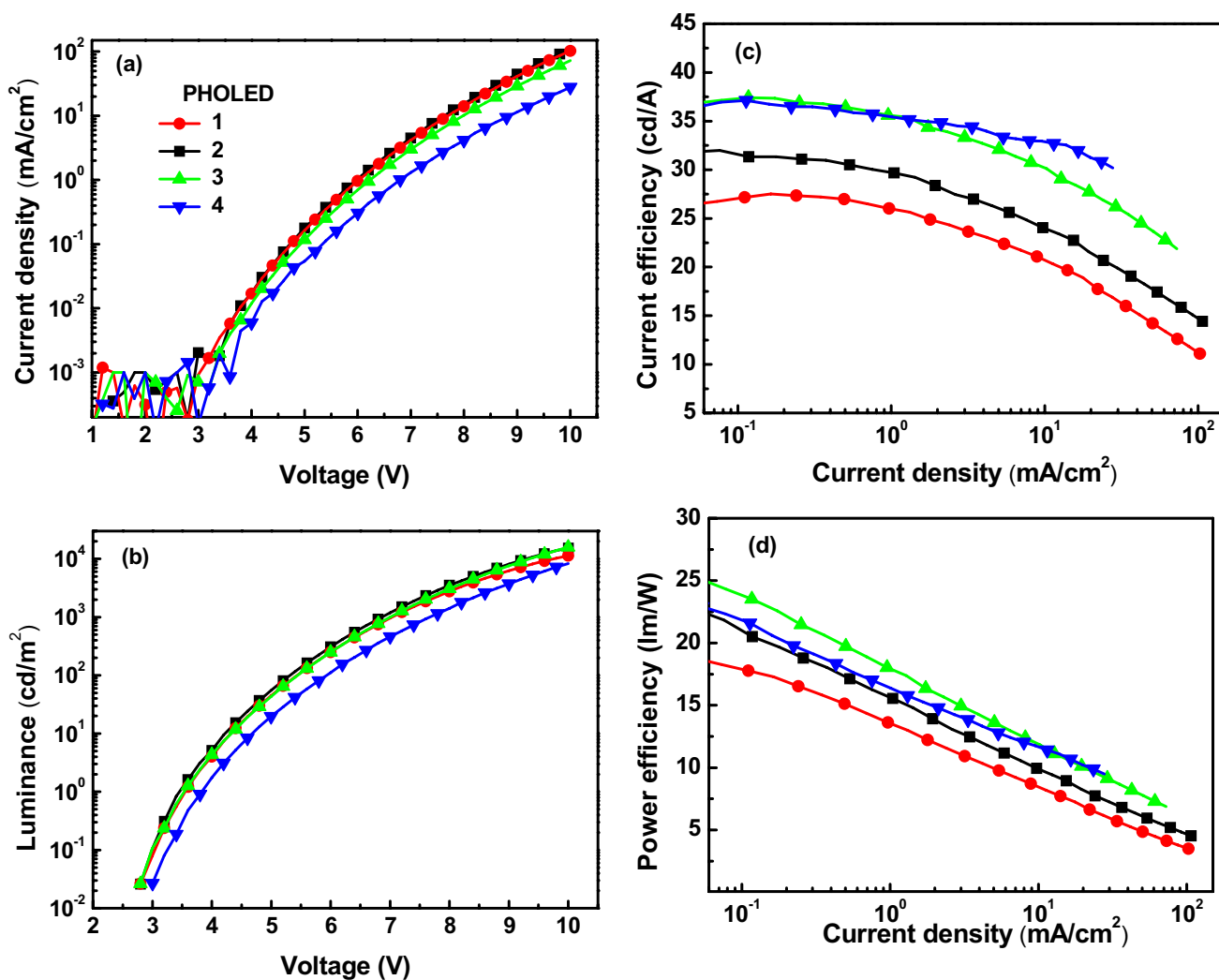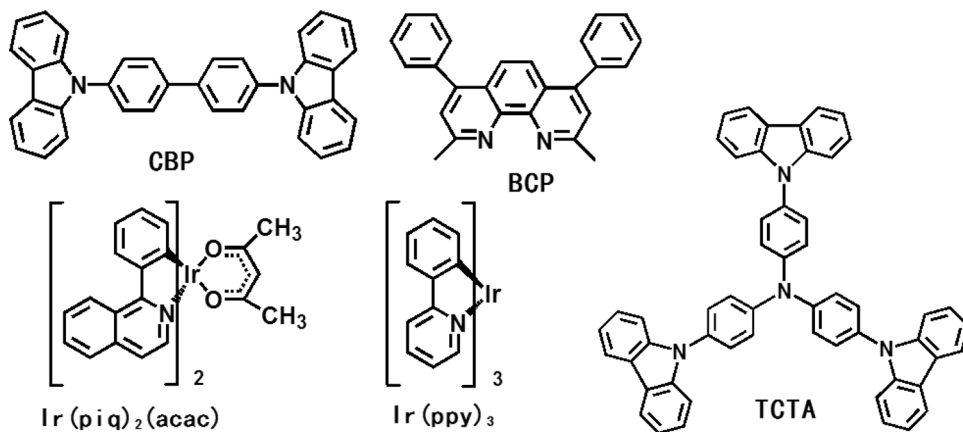**Fig. 1** The molecular structures for CBP, TCTA, BCP, Ir(ppy)$_3$, and Ir(piq)$_2$(acac)

Fig. 2 The *J–V* (**a**), luminance-voltage (**b**), current efficiency-current density (**c**), and power efficiency-current density characteristics (**d**) of PHOLEDs 1–4. The EL spectra of these four devices are shown in Fig. S1

Fig. 3 The normalized EL spectra of PD-BE 1–4 at various driving voltages. The appreciable Ir(ppy)$_3$ emissions for PD-BEs 3 and 4 at high driving voltage are because some excitons diffuse away from the exciton formation zone, thereby avoiding being quenched by Ir(piq)$_2$(acac)
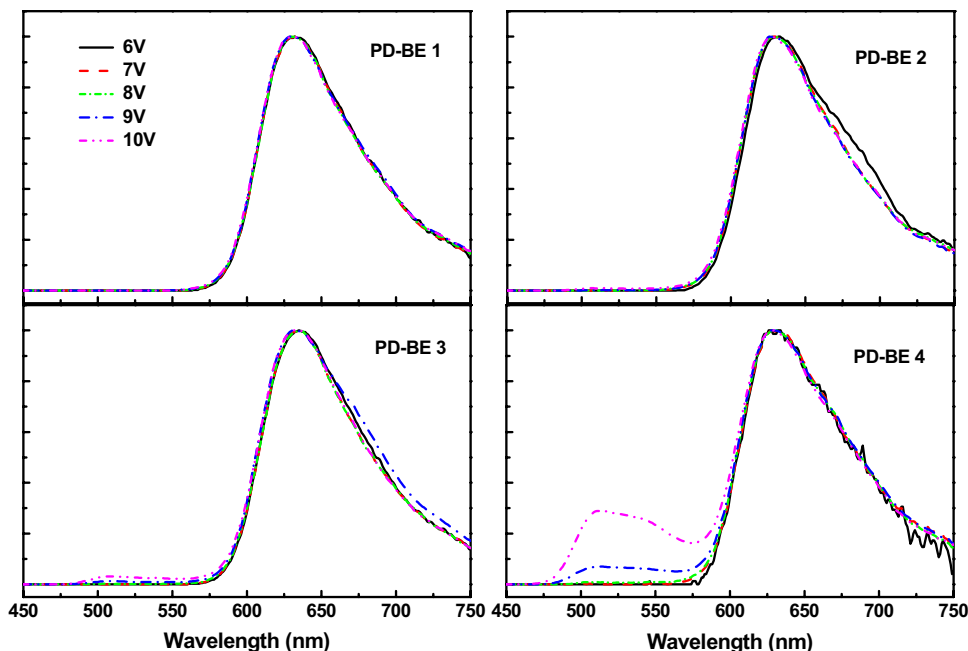
3.2 The determination of *W* in the PHOLEDs 1–4

As shown in Fig. 3, the EL spectra of PD-BEs 1–4 mostly contain Ir(piq)$_2$(acac) emission peaking at 627 nm (Fig. S2), implying that Ir(piq)$_2$(acac) quenches most of the Ir(ppy)$_3$ emissions peaking at 511 nm. This demonstrates the exciton formation zone locates very close to the interface of CBP:Ir(ppy)$_3$ and BCP in PHOLEDs 1–4 [11], likely because the ohmic loss of hole caused by 30 nm

CBP:MoO$_3$/10 nm TCTA is much less than that of electron caused by 50 nm BCP. Figure 4 displays that the EL spectra of PD-TEs 1 and 2 possess both Ir(ppy)$_3$ and Ir(piq)$_2$(acac) emissions, and the relative intensity of Ir(ppy)$_3$ emission to Ir(piq)$_2$(acac) emission for these two devices increases with increase in *V*. This indicates that a certain number of the excitons are directly formed in Ir(piq)$_2$(acac) molecules [5, 6, 21, 22], implying that the *W* equals *x* in PHOLEDs 1 and 2. The EL spectra of PD-TEs 3 and 4 also consist of Ir(ppy)$_3$

Fig. 4 The normalized EL spectra of PD-TE 1–4 at various driving voltages. The green solid line (Ir(ppy)$_3$ emission from PHOLED 4) is shown as reference in the panel of PD-TE 4
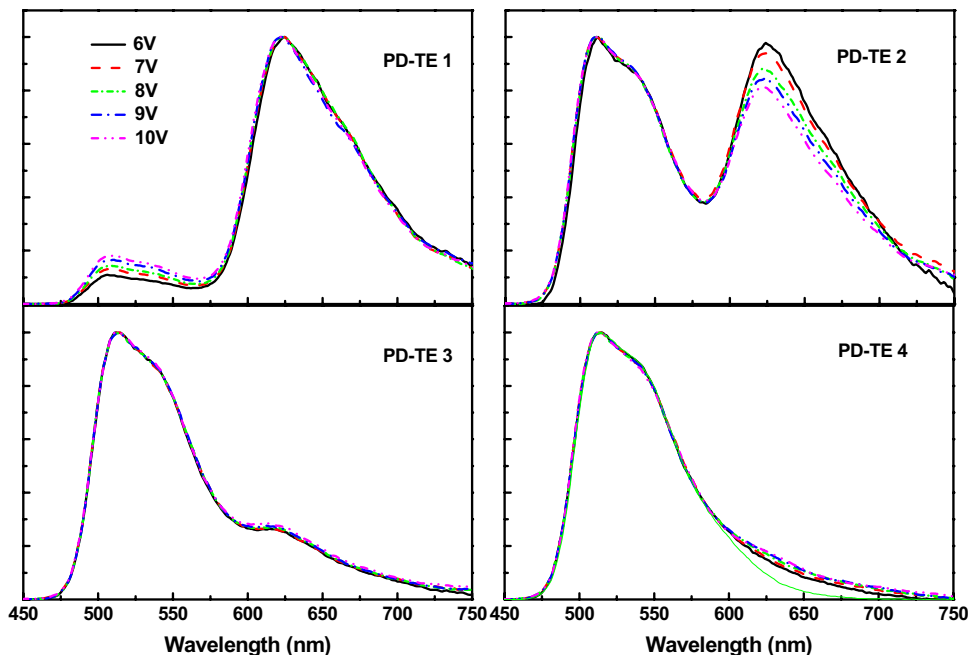
and Ir(piq)$_2$(acac) emissions, but remain almost unchanged with increase in V. This means that the Ir(piq)$_2$(acac) emission mainly results from the energy transfer from Ir(ppy)$_3$ to Ir(piq)$_2$(acac) [1, 4], suggesting that the W is smaller than x in PHOLEDs 3 and 4. The relative intensity of Ir(piq)$_2$(acac) emission to Ir(ppy)$_3$ emission in PHOLED 4 is smaller than that in PHOLED 3, demonstrating that the Ir(piq)$_2$(acac) is further away from to the exciton formation zone in PHOLED 4 than in PHOLED 3.

The concentration of triplet excitons [$^3M^*$] in PHOLED is determined by the rate of triplet electrical generation, and the rates of monoexcitonic recombination and triplet–triplet annihilation (TTA) [23], viz.,

$$\frac{d[^3M^*]}{dt} = -\frac{[^3M^*]}{\tau} - \frac{1}{2}k_{TT}[^3M^*]^2 + \frac{J}{qW}, \tag{2}$$

where τ is the phosphorescent recombination lifetime, k_{TT} is the rate constant of TTA, q is the electron charge, and W is the width of the exciton formation zone. The EQE can be calculated from the steady-state solution of Eq. (2) to give

$$\frac{EQE}{EQE_0} = \frac{J_0}{4J}\left(\sqrt{1 + 8\frac{J}{J_0}} - 1\right), \tag{3}$$

where EQE$_0$ is the quantum efficiency in the absence of TTA, and

$$J_0 = \frac{4qW}{k_{TT}\tau^2}. \tag{4}$$

The EQE and EQE$_0$ can be substituted by CE and CE$_0$, respectively, in Eq. (3). Thus, when $J \leq 1.5$ mA/cm^2, Eq. (3) is simplified via second-order Maclaurin series to be

$$CE = CE_0 - \frac{2CE_0}{J_0}J. \tag{5}$$

The simulations based on Eq. (5) for PHOLEDs 2–4 are shown in Fig. 5. The J_0 for PHOLEDs 2–4 is calculated to 36.4, 41.4, and 49.3 mA/cm^2, respectively. Assuming τ and k_{TT} are constant and taking the values of W and J_0 of PHOLED 2, the W for PHOLEDs 3 and 4 is then calculated to be 5.7 and 6.8 nm, respectively, based on Eq. (4). *Note that*, the W for the EMLs of TCTA:Ir(ppy)$_3$ and *N,N′*-di(naphthalen-2-yl)-*N,N′*-diphenyl-benzidine doped with tris(1-phenylisoquinoline)iridium(III) is estimated below 5 nm via inserting a fluorescent sensitizer into EML [24].

The CE increases in the order of PHOLED 1 < 2 < 3 at a given J, confirming that widening the exciton formation zone can promote the device efficiency [18, 19]. The CEs for PHOLEDs 3 and 4 are almost identical in the low-J range, although the W of PHOLED 3 is smaller than that of PHOLED 4. Nevertheless, the CE of PHOLED 4 slight increases over that of PHOLED 3 at high-J range,
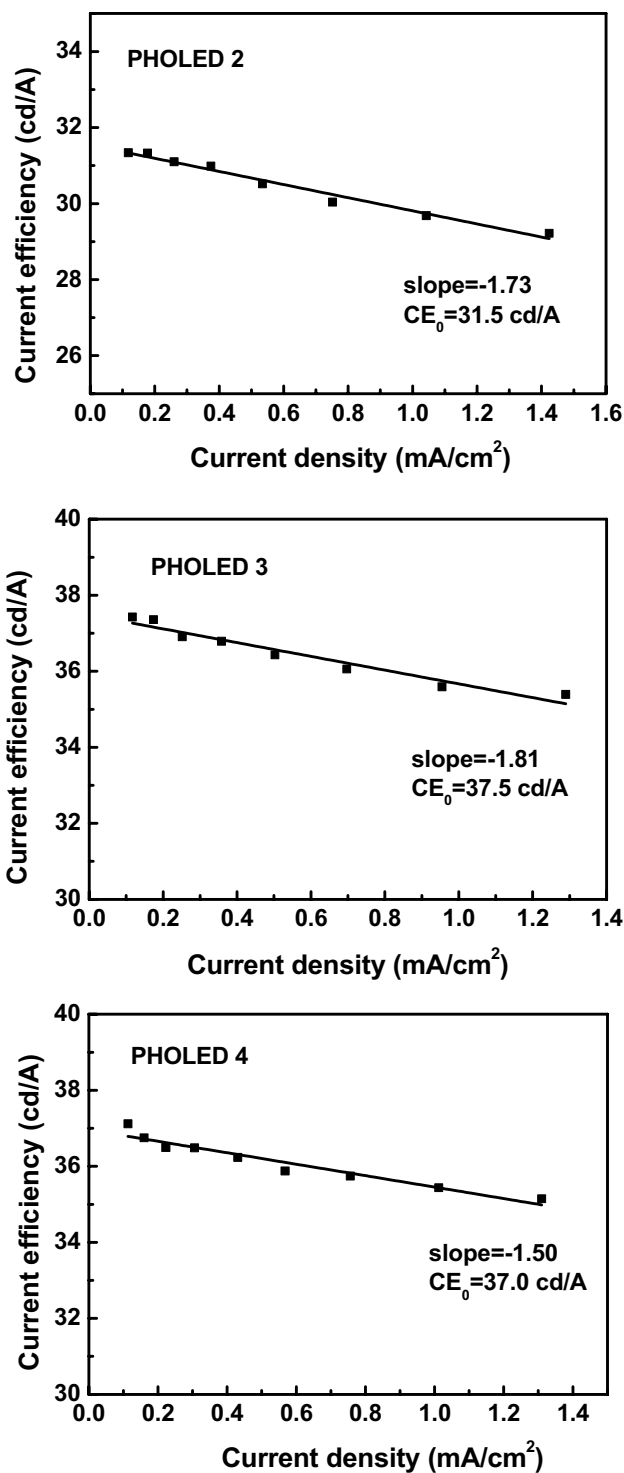

Fig. 5 The linear fits for the current efficiency-current density curves for PHOLEDs 2–4 between 0.1 and 1.5 mA/cm^2. The solid lines are the model calculation according to Eq. (5). The slope of fitted line equals $-2CE_0/J_0$. Thus, the J_0 for PHOLEDs 2–4 is calculated to be 36.4, 41.4, and 49.3 mA/cm^2, respectively. In the range from 0.1 to 1.5 mA/cm^2, the triplet-polaron annihilation is neglected
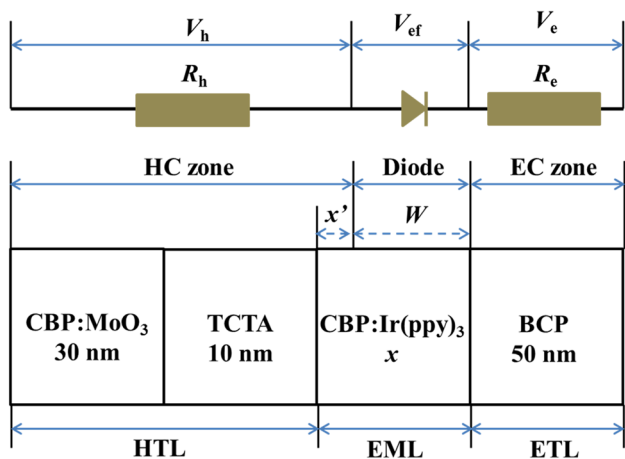
in accordance with the relative intensity of Ir(ppy)$_3$ emission to Ir(piq)$_2$(acac) emission for PD-BE 4 higher than that for PD-BE 3 (Fig. 3), mostly because the TTA gets some relieved in the wider exciton formation zone.

3.3 The electrical properties of the PHOLEDs 1–4

The equivalent circuit for PHOLEDs 1–4 is given in Scheme 1. The voltage drop (V_{ef}) across the exciton formation zone is estimated via Shockley ideal equation

$$J = J_{BR}\left[\exp\left(\frac{qV_{ef}}{k_B T}\right) - 1\right], \tag{6}$$

where J_{BR} is the background current density due to bimolecular recombination and proportional to W, k_B is the Boltzmann constant, and T is the temperature. The voltage drops across HTL (V_h) and ETL (V_e) need to be considered when $J \geq 0.01$ mA/cm^2 [25, 26]. Based on Eq. (6) and the W of PHOLEDs 1 and 2, the V_{ef} for PHOLED 2 is calculated about 0.02 V less than that for PHOLED 1 at a given J. Because the W equals x for PHOLEDs 1 and 2, these two devices have same HC and same EC zones, thereby possessing nearly same V_h and same V_e at a given J. Hence, PHOLED 2 offers slightly decreased V than PHOLED 1 at a given J (Fig. S3). In PHOLEDs 3 and 4, because of $x' = (x-W) > 0$ nm, some part of the EML accommodates no exciton formation and then plays a role of HTL to retard hole current. As a result, PHOLEDs 3 and 4 present markedly increased R_h and V_h and thereby deteriorated J–V curves, relative to PHOLEDs 1 and 2, regardless of their slightly decreased V_{ef}. It is worth noting that the V_e remains nearly invariable for these four devices at a given J, due to the same R_e. Compared to PHOLED 4, PHOLED 3 provides smaller x' and thereby decreased R_h and V_h, improving its J–V curve.

The γ should be same for PHOLEDs 1–4, especially at low J, because of their almost identical layer stacks. Therefore, the CE is thought to be dominated by W. With a given set of HTL and ETL, the W can be enlarged by increasing x, as a result that the ohmic losses of hole and electron become gradually balanced. If $x' = (x-W)$ becomes larger, the V increases significantly, thereby decreasing power efficiency. Based on Scheme 1, the following two requirements should be met in order to achieve high-performance PHOLEDs: (1) to minimize the ohmic losses based on HTL and ETL, reducing V_h and V_e; (2) to balance the ohmic losses based on HTL and ETL, decreasing x' and increasing W at the same time.

4 Conclusions

The variation in current efficiency with the thickness of emissive layer has been investigated for PHOLEDs. It is found that the current efficiency is governed by the width of exciton formation zone that increases with the increase in the thickness of emissive layer. The width of exciton formation zone is measured to be 2.5, 5, 5.7, and 6.8 nm when the thickness of CBP:Ir(ppy)$_3$ emissive layer is 2.5, 5, 10, and 20 nm, respectively. The optimization of the width of exciton formation zone also benefits the improvement in power efficiency. The current research contributes to the design of high-efficiency and low-driving voltage PHOLEDs toward the commercial applications requiring high luminance and long-term stability.

Scheme 1 The equivalent circuit for PHOLEDs 1–4. The HC and EC signify hole and electron current, respectively. The R_h represents the ohmic loss of hole across the HC zone, and V_h signifies the voltage drop across the HC zone at a given J. The R_e denotes the ohmic loss of electron across the EC zone, and V_e means the voltage drop across the EC zone at a given J. The diode indicates the exciton formation zone in emissive layer, and V_{ef} describes the voltage drop across the exciton formation zone. It is pointed out that $V = V_h + V_{ef} + V_e$

References

1. S. Reineke, F. Lindner, G. Schwartz, N. Seidler, K. Walzer, B. Lüssem, K. Leo, Nature **459**, 234 (2009)
2. S. Reineke, M. Thomschke, B. Lüssem, K. Leo, Rev. Mod. Phys. **85**, 1245 (2013)
3. M.K. Fung, Y.Q. Li, L.S. Liao, Adv. Mater. **28**, 10381 (2016)
4. N. Sun, Q. Wang, Y.B. Zhao, Y.H. Chen, D.Z. Yang, F.C. Zhao, J.S. Chen, D.G. Ma, Adv. Mater. **26**, 1617 (2014)
5. Y. Sun, S.R. Forrest, Appl. Phys. Lett. **91**, 263503 (2007)
6. D.S. Qin, Y. Tao, Appl. Phys. Lett. **86**, 113507 (2005)
7. X.K. Chen, Y. Tsuchiya, Y. Ishikawa, C. Zhong, C. Adachi, J.L. Brédas, Adv. Mater. **29**, 1702767 (2017)

8. H. Uoyama, K. Goushi, K. Shizu, H. Nomura, C. Adachi, Nature **492**, 234 (2012)
9. W. Zhao, Z.H. Shi, H. Cao, L. Chen, D.S. Qin, Thin Solid Films **642**, 333 (2017)
10. D.S. Qin, L. Chen, S. Jin, Y.H. Chen, B.B. He, Appl. Phys. A **122**, 72 (2016)
11. N.C. Giebink, S.R. Forrest, Phys. Rev. B **77**, 235215 (2008)
12. C. Coburn, S.R. Forrest, Phys. Rev. Appl. **7**, 041002 (2017)
13. T.D. Schmidt, D.S. Setz, M. Flämmich, J. Frischeisen, D. Michaelis, B.C. Krummacher, N. Danz, W. Brütting, Appl. Phys. Lett. **99**, 163302 (2011)
14. K.H. Kim, S. Lee, C.K. Moon, S.Y. Kim, Y.S. Park, J.H. Lee, J.W. Lee, J. Huh, Y. You, J.J. Kim, Nat. Commun. **5**, 4769 (2014)
15. H. Shin, J.H. Lee, C.K. Moon, J.S. Huh, B. Sim, J.J. Kim, Adv. Mater. **28**, 4920 (2016)
16. D.L. Zhou, W.P. To, Y. Kwak, Y. Cho, G. Cheng, G.S.M. Tong, C.M. Che, Adv. Sci. **6**, 1802297 (2019)
17. Y.W. Zhang, D.D. Zhang, J.B. Wei, Z.Y. Liu, Y. Lu, L. Duan, Angew. Chem. **58**, 17068 (2019)
18. X. Zhou, D.S. Qin, M. Pfeiffer, J. Blochwitz-Nimoth, A. Werner, J. Drechsel, B. Maennig, K. Leo, M. Bold, P. Erk, H. Hartmann, Appl. Phys. Lett. **81**, 4070 (2002)
19. D.S. Qin, Y. Tao, J. Appl. Phys. **97**, 044505 (2005)
20. C. Adachi, R. Kwong, S.R. Forrest, Org. Electron. **2**, 37 (2001)
21. S.H. Shih, J.H. Jou, S.D. Chavhan, T.H. Su, C.H. Yuan, J.W. Wen, P.R. Chen, F.C. Tung, Y.C. Tasi, J. Mater. Chem. C **7**, 15322 (2019)
22. G. Li, J. Shinar, Appl. Phys. Lett. **83**, 5359 (2003)
23. M.A. Baldo, C. Adachi, S.R. Forrest, Phys. Rev. B **62**, 10967 (2000)
24. S. Reineke, K. Walzer, K. Leo, Phys. Rev. B **75**, 125328 (2007)
25. A. Fischer, M. Pfalz, K. Vandewal, S. Lenk, M. Liero, A. Glitzky, S. Reineke, Phys. Rev. Applied **10**, 014023 (2018)
26. P.E. Burrows, S.R. Forrest, Appl. Phys. Lett. **64**, 2285 (1994)